

Kinetics of epoxidation of cyclooctene with H_2O_2 by α -Keggin $[\text{PTi}_2\text{W}_{10}\text{O}_{38}(\text{O}_2)_2]^{7-}$ catalyst in acetonitrile

Eri Ishikawa, Toshihiro Yamase *

Research Laboratory of Resources Utilization, Tokyo Institute of Technology, 4259 Nagatsuta Midori-ku, Yokohama 226-8503, Japan

Received 19 March 1998; accepted 4 August 1998

Abstract

$\text{Ti}(\eta^2\text{-O}_2)\text{O}_5$ and adjacent W sites in α -Keggin $[\text{PTi}_2\text{W}_{10}\text{O}_{38}(\text{O}_2)_2]^{7-}$ synergistically catalyze cyclooctene epoxidation and H_2O_2 dismutation in the monophasic $[\text{PTi}_2\text{W}_{10}\text{O}_{38}(\text{O}_2)_2]^{7-}/\text{H}_2\text{O}_2/\text{CH}_3\text{CN}$ system. The alkene coordination to the $\text{Ti}(\eta^2\text{-O}_2)\text{O}_5$ site precedes the epoxidation, and the decomposition of $[\text{PTi}_2\text{W}_{10}\text{O}_{38}(\text{O}_2)_2]^{7-}$ by self-oxidation throughout the reactions is minor. From the kinetic results of the reactions it is inferred that the reaction pathway of the catalyst with H_2O_2 is altered by the alkene coordination to the $\text{Ti}(\eta^2\text{-O}_2)\text{O}_5$ site as an active site for the H_2O_2 dismutation, which modifies the electronic structure of surrounding sites, resulted in an active site for the epoxidation with an involvement of peroxy catalyst intermediates. © 1999 Elsevier Science B.V. All rights reserved.

Keywords: Peroxo Keggin-type Ti-substituted polyoxotungstate; Alkene epoxidation; Reaction kinetics; Alkene coordination to catalyst; H_2O_2 dismutation; ^{31}P NMR

1. Introduction

Earlier we reported the catalytic activity of the aryldiazonium salts of Ti-substituted Keggin-type polyoxotungstates $[\text{PTi}_x\text{W}_{12-x}\text{O}_{40}]^{(3+2x)-}$ and $[\text{PTi}_x\text{W}_{12-x}\text{O}_{40-x}(\text{O}_2)_x]^{(3+2x)-}$ ($x = 1$ and 2) for the alkene epoxidation by H_2O_2 (alkene + $\text{H}_2\text{O}_2 \rightarrow$ alkene epoxide + H_2O) in acetonitrile/dichloromethane (1/1, v/v) [1]. The results indicated that η^2 -peroxidation at TiO_6 octahedron sites in $[\text{PTi}_x\text{W}_{12-x}\text{O}_{40}]^{(3+2x)-}$ by H_2O_2 to $[\text{PTi}_x\text{W}_{12-x}\text{O}_{40-x}(\text{O}_2)_x]^{(3+2x)-}$ ($x = 1$ and 2) is followed by the alkene epoxidation due to a synergistic effect of the $\text{Ti}(\eta^2\text{-peroxo})$ site with a neighboring W site. There are also many reports of oxidation processes catalyzed by other polyoxometalates: early transition metal (such as Cr^{III} , Co^{II} , Mn^{II} , Fe^{II} , Ni^{II} , and Cu^{II}) substituted Keggin-structural polyoxometalates (TMSP) are known to catalyze the alkene oxidation to epoxide with aqueous H_2O_2 without degradation of the catalysts [2–5]. The stable feature of TMSP throughout the reaction is unique, although definitive mechanistic work is lacking. Recently sandwich-type TMSPs in which four transition-metal ions link two trivacant Keggin and Wells-Dawson fragments as TMSPs of other

* Corresponding author. Tel.: +81-45-9245260; Fax: +81-45-9245276; E-mail: tyamase@res.titach.ac.jp

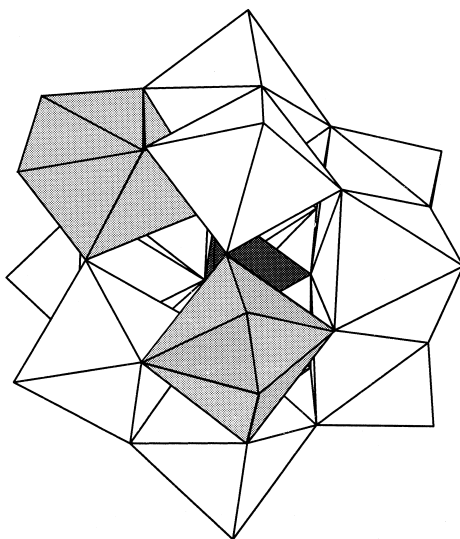


Fig. 1. Coordination polyhedra representation of $[\text{PTi}_2\text{W}_{10}\text{O}_{38}(\text{O}_2)_2]^{7-}$. The black tetrahedron is PO_4^{3-} , the gray decahedra represent Ti, and the remaining white octahedra are W.

structural classes, $[(\text{TM}^{\text{II}})_4(\text{H}_2\text{O})_2(\text{PW}_9\text{O}_{34})_2]^{10-}$ (TM = Co, Fe) [6], $[\text{WZnTM}^{\text{II}}(\text{ZnW}_9\text{O}_{34})_2]^{12-}$ (TM = Mn, Pd, Pt) [7,8], $[\text{WZnRu}^{\text{III}}(\text{ZnW}_9\text{O}_{34})_2]^{10-}$ [8], $[\text{Fe}_4^{\text{II}}(\text{H}_2\text{O})_2(\text{P}_2\text{W}_{15}\text{O}_{56})_2]^{16-}$ [6], and $[\text{Fe}_4^{\text{III}}(\text{H}_2\text{O})_2(\text{P}_2\text{W}_{15}\text{O}_{56})_2]^{12-}$ [9], were also used. However, until now, less is known in these cases about the nature of the active catalyst. The only catalyst of structurally well-characterized polyoxometalate is $[(\text{PO}_4)\text{W}_4\text{O}_4(\text{O}_2)_8]^{3-}$ which comprises both terminal η^2 and bridging ($\eta^2:\eta^1$) peroxo ligands [10] and is formed in the reaction pathway between $\text{H}_3[\text{PW}_{12}\text{O}_{40}]$ and H_2O_2 under biphasic conditions of chlorinated solvents [11–19]. In order to discuss the nature of the active intermediates involved in the alkene epoxidation, we report here kinetics of the epoxidation of cyclooctene for the $[\text{PTi}_2\text{W}_{10}\text{O}_{38}(\text{O}_2)_2]^{7-}/\text{H}_2\text{O}_2/\text{CH}_3\text{CN}$ monophasic system where the cyclooctene coordination to the $\text{Ti}(\eta^2\text{-O}_2)\text{O}_5$ site precedes and the epoxidation proceeds with retention of the Keggin structure of catalyst.

$[\text{Pr}^{\text{I}}\text{NH}_3]_6\text{H}[\text{PTi}_2\text{W}_{10}\text{O}_{38}(\text{O}_2)_2] \cdot \text{H}_2\text{O}$ has been characterized by X-ray diffractometry and ^{31}P and ^{183}W NMR spectroscopy. Fig. 1 shows the structure of $[\text{PTi}_2\text{W}_{10}\text{O}_{38}(\text{O}_2)_2]^{7-}$, indicating that two $\text{Ti}(\eta^2\text{-O}_2)\text{O}_5$ sites are located in C_2 -symmetric relationship for the α -Keggin tungstophosphate framework [20]. The $[\text{NBu}_4]^+$ salt of $[\text{PTi}_2\text{W}_{10}\text{O}_{38}(\text{O}_2)_2]^{7-}$ in this study is employed for its high solubility in CH_3CN .

2. Experimental

$[\text{NBu}_4]_3[\text{PW}_{12}\text{O}_{40}]$ [1], $[\text{NBu}_4]_5\text{K}_2[\text{PTi}_2\text{W}_{10}\text{O}_{40}] \cdot 6 \text{H}_2\text{O}$ [1], $\text{K}_7[\text{PTi}_2\text{W}_{10}\text{O}_{40}] \cdot 6 \text{H}_2\text{O}$ [21], and $[\text{Pr}^{\text{I}}\text{NH}_3]_6\text{H}[\text{PTi}_2\text{W}_{10}\text{O}_{38}(\text{O}_2)_2] \cdot \text{H}_2\text{O}$ [20] were prepared and identified according to published procedures. IR spectra agreed with those reported for corresponding compounds. $[\text{NBu}_4]_4[\text{Pr}_2^{\text{I}}\text{NH}_2]_2\text{-H}[\text{PTi}_2\text{W}_{10}\text{O}_{38}(\text{O}_2)_2] \cdot 2 \text{H}_2\text{O}$ was prepared by adding $[\text{NBu}_4]\text{Br}$ (0.8 g) into an aqueous solution (4 ml) of $[\text{Pr}^{\text{I}}\text{NH}_3]_6\text{H}[\text{PTi}_2\text{W}_{10}\text{O}_{38}(\text{O}_2)_2] \cdot \text{H}_2\text{O}$ (1 g) and adjusting a resulting solution to pH 5.0. Yellow precipitate was filtered off, washed with water, and dried (Found: C, 23.08; H, 4.55; N, 1.85. Calculation for $\text{C}_{72}\text{H}_{181}\text{N}_6\text{O}_{44}\text{PTi}_2\text{W}_{10}$: C, 23.72; H, 4.79; N, 2.18%). 60% aqueous H_2O_2 was

generously provided from Mitsubishi Gas Chemical Company. All other reagents were at least analytical grade and were used as supplied.

Catalytic oxidation reactions of alkene by H_2O_2 were carried out in a 30-ml round-bottomed flask, which was charged with $[\text{NBu}_4]_4[\text{Pr}_2^{\text{i}}\text{NH}_2]_2\text{H}[\text{PTi}_2\text{W}_{10}\text{O}_{38}(\text{O}_2)_2] \cdot 2 \text{H}_2\text{O}$ catalyst, 60% aqueous H_2O_2 , and cyclooctene in 30 ml CH_3CN . The reaction vessel with a stirring magnetic bar was connected with a -5°C -ethanol/water (1/3, v/v)-cooled reflux condenser capped with a glass stopper to minimize the vapor pressure of CH_3CN during the reaction which was initiated by degassing 20 ml of the head space and adding various amounts of cyclooctene and 60% H_2O_2 via syringe at 69°C under reflux conditions. Aliquots (1 μl) of the monophasic sample solution were removed and analyzed by GC. The epoxide was identified and quantified by GC-MS and GC. The head space atmosphere was analyzed by withdrawing gas aliquots (2 ml) via a gas-tight syringe. Oxygen was identified by coinjection of an authentic sample. Oxygen was quantified using nitrogen from air as an internal standard (subtracting the corresponding moles of O_2 in air). The oxygen content in the sample solution was not taken into consideration for the generated oxygen. The rates of epoxide and oxygen generation were determined using the initial rate method. The insertion of syringe into both reaction vessel and its head space was done through the septum stoppers.

The amount of crystal water was determined by thermogravimetric analysis (Sinku-Riko MTS-9000 + TGD-9600). IR and electronic spectra were recorded on JASCO FT/IR-5000 and Hitachi 330 spectrometers, respectively. The NMR spectra was obtained on a JEOL GSX-270 spectrometer (^{31}P , 109.4 MHz) as CD_3CN or D_2O solutions, using external H_3PO_4 as reference. The amount of hydrocarbon derivatives and dioxygen before and after reactions were determined by GC (on a GL Science GL-353 instrument with a TC-WAX capillary 30-m column for the former and a Hitachi 164 GC with a molecular sieve 5A 1-m column for the latter). GC-MS data on Hitachi M80 GC/MS spectrometer with PEG-20 M column were used for the identification of the oxidation products. Cyclic voltammograms were measured with a potentiostat/galvanostat (Hokuto Denko HA-301) and a function generator (Nikko Keisoku NFG-3). The sample solution containing 1.0 mM $[\text{NBu}_4]_4[\text{Pr}_2^{\text{i}}\text{NH}_2]_2\text{H}[\text{PTi}_2\text{W}_{10}\text{O}_{38}(\text{O}_2)_2] \cdot 2 \text{H}_2\text{O}$ and 0.1 M LiClO_4 in CH_3CN were purged with argon and measured using a carbon-fiber (33 μm diameter) working electrode, a platinum-wire counter electrode, and a Ag-wire reference electrode. After each measurement the working electrode was polished with 0.3- μm Al_2O_3 (Buehler) and rinsed with water to ensure reproducible results. All electric potentials quoted are with reference to Ag/AgCl (saturated KCl) electrode.

3. Results and discussion

3.1. Interaction between $[\text{PTi}_2\text{W}_{10}\text{O}_{38}(\text{O}_2)_2]^{7-}$ and cyclooctene

Solutions of $[\text{Bu}_4\text{N}]_4[\text{Pr}^{\text{i}}\text{NH}_3]_2\text{H}[\text{PTi}_2\text{W}_{10}\text{O}_{38}(\text{O}_2)_2] \cdot 2 \text{H}_2\text{O}$ in CH_3CN show absorption bands at 262 nm ($\varepsilon = 5.03 \times 10^4 \text{ M}^{-1} \text{ cm}^{-1}$) and 398 nm ($\varepsilon = 3.88 \times 10^3 \text{ M}^{-1} \text{ cm}^{-1}$), which are assigned to the $\text{O} \rightarrow \text{W}$ and $\eta^2\text{-O}_2 \rightarrow \text{Ti}$ ligand-to-metal charge transfer bands, respectively. Addition of cyclooctene into the $[\text{Bu}_4\text{N}]_4[\text{Pr}^{\text{i}}\text{NH}_3]_2\text{H}[\text{PTi}_2\text{W}_{10}\text{O}_{38}(\text{O}_2)_2] \cdot 2 \text{H}_2\text{O}$ solution results in decrease of absorbance without appearance of other absorption to reach depressed values, as shown in Fig. 2. In contrast, $[\text{Bu}_4\text{N}]_4\text{K}_2\text{H}[\text{PTi}_2\text{W}_{10}\text{O}_{40}] \cdot 6 \text{H}_2\text{O}$, showing a single absorption maximum at 262 nm ($\varepsilon = 4.50 \times 10^4 \text{ M}^{-1} \text{ cm}^{-1}$) in CH_3CN , exhibits no significant change of the absorbance in the presence of cyclooctene, as shown in Fig. 2(B). ^{31}P NMR spectra were taken of a mixture in which five equivalents of cyclooctene was added to a 30 mM solution of $[\text{Bu}_4\text{N}]_4[\text{Pr}^{\text{i}}\text{NH}_3]_2\text{H}[\text{PTi}_2\text{W}_{10}$ -

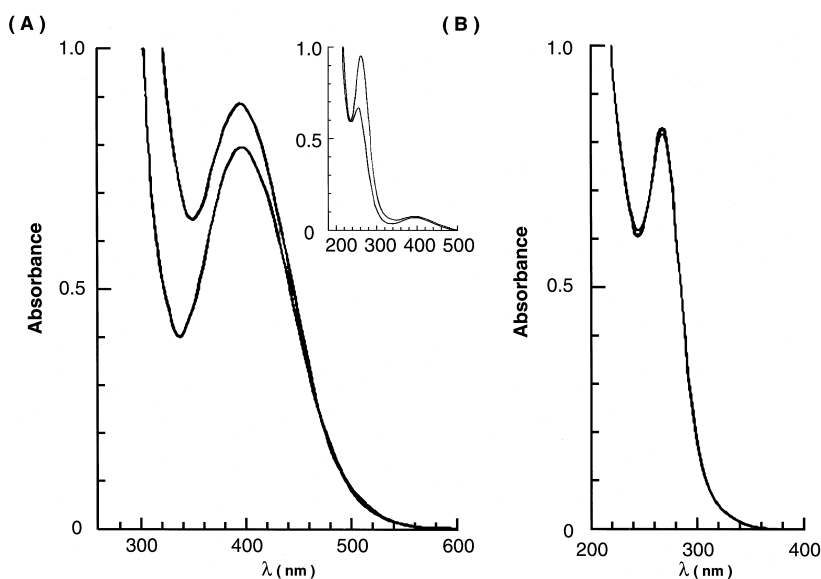


Fig. 2. UV-visible spectra of 0.2 mM $[\text{Bu}_4\text{N}]_4[\text{Pr}^1\text{NH}_3]_2\text{H}[\text{PTi}_2\text{W}_{10}\text{O}_{38}(\text{O}_2)_2] \cdot 2 \text{H}_2\text{O}$ (A) in CH_3CN before (top) and after (bottom) addition of 10 mM cyclooctene; insert: spectral changes at 200–350 nm for 0.02 mM $[\text{Bu}_4\text{N}]_4[\text{Pr}^1\text{NH}_3]_2\text{H}[\text{PTi}_2\text{W}_{10}\text{O}_{38}(\text{O}_2)_2] \cdot 2 \text{H}_2\text{O}$ before (top) and after (bottom) addition of 1 mM cyclooctene. UV spectrum of 0.02 mM $[\text{Bu}_4\text{N}]_4\text{K}_2\text{H}[\text{PTi}_2\text{W}_{10}\text{O}_{40}] \cdot 6 \text{H}_2\text{O}$ (B) in CH_3CN was hardly changed by the addition of cyclooctene. Optical pathlength for every measurement is 10 mm.

$\text{O}_{38}(\text{O}_2)_2] \cdot 2 \text{H}_2\text{O}$ in CD_3CN . As shown in Fig. 3, the resulting ^{31}P NMR spectrum (Fig. 3(B)) shows primarily a broad resonance (with a half-width of $\nu_{1/2} = 57.0$ Hz) at $\delta -10.8$ and is similar to the spectrum at $\delta -10.7$ with $\nu_{1/2} = 36.0$ Hz (Fig. 3(A)) of $[\text{Bu}_4\text{N}]_4[\text{Pr}^1\text{NH}_3]_2\text{H}[\text{PTi}_2\text{W}_{10}\text{O}_{38}(\text{O}_2)_2] \cdot 2 \text{H}_2\text{O}$ which shows at least 90% of a single species and isomer. This result indicates that there is no significant fragmentation of the catalyst during the reaction with cyclooctene. In Fig. 3(C), the ^{31}P NMR spectrum (at $\delta -11.4$ with $\nu_{1/2} = 6.7$ Hz irrespective of the presence of cyclooctene) of

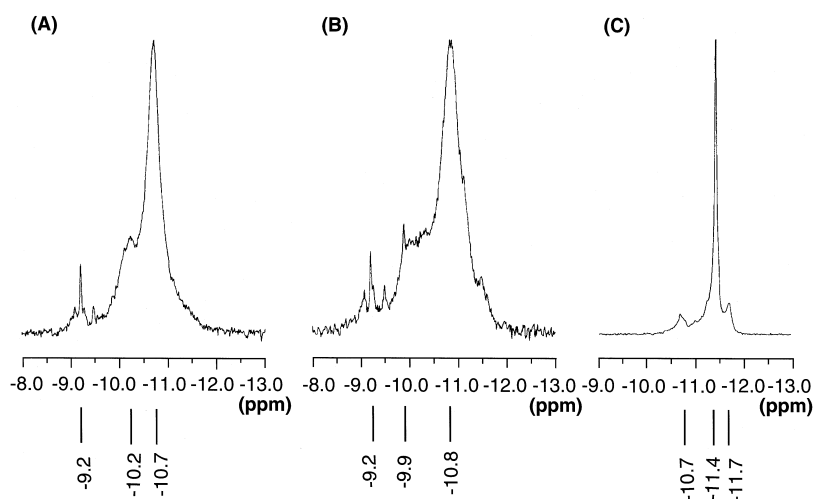
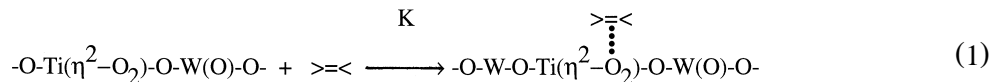
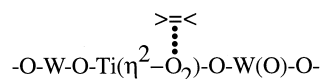


Fig. 3. ^{31}P NMR spectra of 30 mM $[\text{Bu}_4\text{N}]_4[\text{Pr}^1\text{NH}_3]_2\text{H}[\text{PTi}_2\text{W}_{10}\text{O}_{38}(\text{O}_2)_2] \cdot 2 \text{H}_2\text{O}$ (A), the coexistence of 0.15 M cyclooctene (B), and 80 mM $[\text{Bu}_4\text{N}]_4\text{K}_2\text{H}[\text{PTi}_2\text{W}_{10}\text{O}_{40}] \cdot 6 \text{H}_2\text{O}$ (C) in CD_3CN .

30 mM $[\text{Bu}_4\text{N}]_4\text{K}_2\text{H}[\text{PTi}_2\text{W}_{10}\text{O}_{40}] \cdot 6 \text{H}_2\text{O}$ in CD_3CN is added for comparison, implying that the coordination of cyclooctene to the $\eta^2\text{-O}_2$ ligand at the Ti site in $[\text{PTi}_2\text{W}_{10}\text{O}_{38}(\text{O}_2)_2]^{7-}$ results in broadening of the ^{31}P NMR line of the compound. Thus, the electronic spectra in Fig. 2(A) indicate that alkenes nucleophilically interact with the $\eta^2\text{-O}_2$ ligand at the Ti site in $[\text{PTi}_2\text{W}_{10}\text{O}_{38}(\text{O}_2)_2]^{7-}$ to generate a distortion of neighboring WO_6 octahedra with a resultant decrease in absorbance, as denoted by Eq. (1):



where $-\text{O}-\text{Ti}(\eta^2\text{-O}_2)\text{-O}-\text{W}(\text{O})\text{-O}-$, >=< , and



indicate the $\text{Ti}(\eta^2\text{-O}_2)\text{O}_5$ site environment of catalyst, cyclooctene, and cyclooctene-coordinated species, respectively. Such a cyclooctene-coordinated species acts as a precursor for the epoxidation by H_2O_2 . The formation constant (K) of the alkene-coordinated species and its absorption coefficients at 398 nm can be obtained from application of Ketelaar's method (plot of the inverse absorbance difference versus inverse alkene concentration) [22] into the absorption spectra of the $[\text{Bu}_4\text{N}]_4[\text{Pr}^i\text{NH}_3]_2\text{H}[\text{PTi}_2\text{W}_{10}\text{O}_{38}(\text{O}_2)_2] \cdot 2 \text{H}_2\text{O}/\text{cyclooctene}/\text{CH}_3\text{CN}$ system, to give $K = 4.04 \times 10^3 \text{ M}^{-1}$ and $\epsilon_{398} = 3.36 \times 10^3 \text{ M}^{-1} \text{ cm}^{-1}$ at room temperature.

The electronic structural change of the catalyst by the alkene coordination may be reflected in the electrochemical processes on the carbon-fiber electrode in CH_3CN . The curve A of Fig. 4 represents the cyclic voltammogram of $[\text{Bu}_4\text{N}]_4[\text{Pr}^i\text{NH}_3]_2\text{H}[\text{PTi}_2\text{W}_{10}\text{O}_{38}(\text{O}_2)_2] \cdot 2 \text{H}_2\text{O}$, which shows two pseudo-reversible peak couples of reductions at -1.28 and -1.70 V and oxidations at -1.16 and -1.44 V, attributed to the $\text{W}(\text{VI})/\text{W}(\text{V})$ and/or $\text{Ti}(\text{IV})/\text{Ti}(\text{III})$ in the anion framework. The second peak couple seems to be composite and broad due to coalescence of two waves which are difficult to decipher. The curve B of Fig. 4 for the addition of 5 mM cyclooctene indicates that the two pseudo-reversible peak couples of reductions at -1.16 and -1.54 V and oxidations at -0.98 and -1.36 V are distinctly about 0.1 V more positive in potential compared to the curve A. The curve C of Fig. 4 shows the peak couples for $[\text{Bu}_4\text{N}]_4\text{K}_2\text{H}[\text{PTi}_2\text{W}_{10}\text{O}_{40}] \cdot 6 \text{H}_2\text{O}$ for comparison. In curve C, the current intensity for the second peak couple of the reduction at -1.16 V and oxidation at -1.00 V is approximately two-fold larger than for the first couple of the reduction at -0.82 V and oxidation at -0.66 V, indicating that the second peak results from coalescence of at least two waves for the reduction of metal sites in the anion framework. The curve C differs from our previous cyclic voltammogram at a hanging mercury electrode for $\text{K}_7[\text{PTi}_2\text{W}_{10}\text{O}_{40}] \cdot 8 \text{H}_2\text{O}$ at $\text{pH} = 5.4$, which consisted of two successive pseudo-reversible one-electron redox waves due to $\text{W}(\text{VI})/\text{W}(\text{V})$ exhibiting reduction peaks at -1.04 and -1.15 V [23]. Turning now to the remaining waves of the cyclic voltammogram of $[\text{Bu}_4\text{N}]_4[\text{Pr}^i\text{NH}_3]_2\text{H}[\text{PTi}_2\text{W}_{10}\text{O}_{38}(\text{O}_2)_2] \cdot 2 \text{H}_2\text{O}$, the reversible wave at about $+0.3$ V may be associated with redox peaks of the $\eta^2\text{-O}_2$ ligand at the Ti site in the anion, since $[\text{Bu}_4\text{N}]_4\text{K}_2\text{H}[\text{PTi}_2\text{W}_{10}\text{O}_{40}] \cdot 6 \text{H}_2\text{O}$ exhibits no wave at the same potential region. As shown on curve B, the coexistence of cyclooctene leads to irreversible oxidation of the $\eta^2\text{-O}_2$ ligand. In conjunction with the broadening of the ^{31}P NMR spectrum (Fig. 3) of $[\text{Bu}_4\text{N}]_4[\text{Pr}^i\text{NH}_3]_2\text{-}$

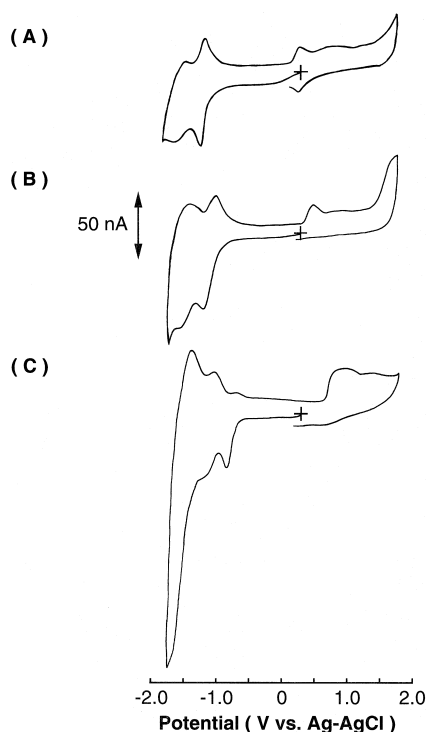


Fig. 4. Comparison of the cyclic voltammograms observed in CH_3CN medium (0.1 M LiClO_4) for 1.0 mM $[\text{Bu}_4\text{N}]_4[\text{Pr}^i\text{NH}_3]_2\text{H}[\text{PTi}_2\text{W}_{10}\text{O}_{38}(\text{O}_2)_2] \cdot 2 \text{H}_2\text{O}$ (curve A), 1.0 mM $[\text{Bu}_4\text{N}]_4[\text{Pr}^i\text{NH}_3]_2\text{H}[\text{PTi}_2\text{W}_{10}\text{O}_{38}(\text{O}_2)_2] \cdot 2 \text{H}_2\text{O}$ and 5 mM cyclooctene (curve B), and 1.0 mM $[\text{Bu}_4\text{N}]_4\text{K}_2\text{H}[\text{PTi}_2\text{W}_{10}\text{O}_{40}] \cdot 6 \text{H}_2\text{O}$ (curve C); scan rate: 100 mV/s.

$\text{H}[\text{PTi}_2\text{W}_{10}\text{O}_{38}(\text{O}_2)_2] \cdot 2 \text{H}_2\text{O}$ in the presence of cyclooctene, thus, the difference in voltammetric patterns between curves A and B reveals that the framework distortion due to the coordination of cyclooctene to the $\eta^2\text{-O}_2$ ligand at the Ti site causes subtle variations in the detailed electronic structure of the anion to alter redox properties.

3.2. Product studies

When the solutions containing $[\text{Bu}_4\text{N}]_4[\text{Pr}^i\text{NH}_3]_2\text{H}[\text{PTi}_2\text{W}_{10}\text{O}_{38}(\text{O}_2)_2] \cdot 2 \text{H}_2\text{O}$, cyclooctene, and 60% H_2O_2 in 30 ml CH_3CN were kept at 69°C for 24 h, cyclooctene oxide and oxygen were main products and cyclooctane 1,2-diol was a minor product. The absence of $[\text{Bu}_4\text{N}]_4[\text{Pr}^i\text{NH}_3]_2\text{H}[\text{PTi}_2\text{W}_{10}\text{O}_{38}(\text{O}_2)_2] \cdot 2 \text{H}_2\text{O}$ resulted in low conversion (< 9% for epoxide at 24 h) to cyclooctene oxide and oxygen. Table 1 lists amounts of products and reactants with a variety of initial concentrations of $[\text{Bu}_4\text{N}]_4[\text{Pr}^i\text{NH}_3]_2\text{H}[\text{PTi}_2\text{W}_{10}\text{O}_{38}(\text{O}_2)_2] \cdot 2 \text{H}_2\text{O}$ (0.07–2.0 mM), cyclooctene (0–1.0 M), and H_2O_2 (0.27–0.93 M). The results for the reaction at 69°C for 24 h indicate that both cyclooctene epoxidation and oxygen evolution stoichiometrically obey reactions (2) and (3), respectively:

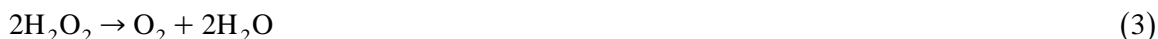
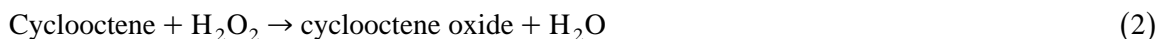




Table 1

Amounts of products and reactants with a variety of initial concentrations of $[\text{Bu}_4\text{N}]_4[\text{Pr}^i\text{NH}_3]_2\text{H}[\text{PTi}_2\text{W}_{10}\text{O}_{38}(\text{O}_2)_2] \cdot 2\text{H}_2\text{O}$ (0.07–2.0 mM), cyclooctene (0–1.0 M) and H_2O_2 (0.27–0.93 M) for the 24-h reaction at 69°C

before reaction			after reaction			
[catalyst] (mM)	 ($\times 10^{-1}$ M)	$[\text{H}_2\text{O}_2]$ ($\times 10^{-1}$ M)	$-\text{[cyclooctene]}$ ($\times 10^{-1}$ M)	 ($\times 10^{-1}$ M)	$[\text{O}_2]$ ($\times 10^{-2}$ M)	$[\text{H}_2\text{O}_2]$ ($\times 10^{-1}$ M)
0.67	2.0	9.33	1.99	1.89	7.83	5.67
		8.0	1.96	1.66	7.90	3.99
		6.67	1.93	1.71	7.83	3.28
		5.33	1.70	1.33	5.37	2.58
		4.0	1.51	1.26	2.90	
		2.67	0.98	0.92	2.10	
0.67	9.33	10.0	8.28	6.27	1.37	1.35
		6.0	5.77	5.01	4.50	
		5.0	4.76	4.17	7.23	
		4.0	3.91	3.55	6.57	3.40
		3.0	2.92	2.60	8.63	
		1.0	0.99	0.82	7.87	6.07
2.0	2.0	9.33	1.86 ^a	1.73 ^a	7.30 ^a	
1.33			1.98 ^b	1.77 ^b	7.60 ^b	
0.33			1.93	1.76	7.30	
0.07			1.85	1.83	6.43	
0.67	0	9.33			11.2	
					8.20	
					9.77	
					8.73	
					3.87	
2.0	0	9.33			8.63 ^c	
1.33					8.53 ^d	
0.33					8.23	
0.67					7.33	

^aFor 9-h reaction.

^bFor 12-h reaction.

^cFor 2-h reaction.

^dFor 3-h reaction.

As represented in Table 1, $[\text{Bu}_4\text{N}]_4[\text{Pr}^i\text{NH}_3]_2\text{H}[\text{PTi}_2\text{W}_{10}\text{O}_{38}(\text{O}_2)_2] \cdot 2\text{H}_2\text{O}$ showed high turnovers of 87–2731 for the selective epoxidation of cyclooctene. Disagreement between amounts of the reacted cyclooctene and the produced epoxide, which is observed especially under the condition of high yield of epoxide, could be attributed mainly to the formation of 1,2-cyclooctanediol as a result of the ring-opening of epoxide [1] and was not further studied. The ratio of amounts of epoxide to oxygen increases with an increase in initial concentration of cyclooctene and decreases with an increase in initial concentration of H_2O_2 , while the ratio is not strongly affected by a variety of amount of $[\text{Bu}_4\text{N}]_4[\text{Pr}^i\text{NH}_3]_2\text{H}[\text{PTi}_2\text{W}_{10}\text{O}_{38}(\text{O}_2)_2] \cdot 2\text{H}_2\text{O}$ catalyst. Fig. 5 shows the time-dependence of the evolution of cyclooctene oxide (A) and oxygen (B) at 69°C for the $[\text{Bu}_4\text{N}]_4[\text{Pr}^i\text{NH}_3]_2\text{H}[\text{PTi}_2\text{W}_{10}\text{O}_{38}(\text{O}_2)_2] \cdot 2\text{H}_2\text{O}$ (0.67 mM)/cyclooctene (0.1–1.0 M)/60% H_2O_2 (0.93 M)/ CH_3CN (30 ml) system. As shown in Fig. 5, there is approximately linear relationship between product

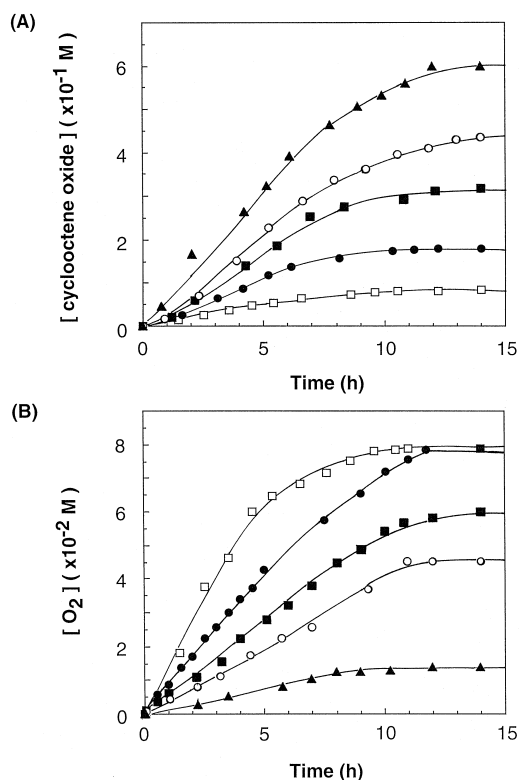


Fig. 5. Time-dependent yields of cyclooctene oxide (A) and oxygen (B) for the $[\text{Bu}_4\text{N}]_4[\text{Pr}^1\text{NH}_3]_2\text{H}[\text{PTi}_2\text{W}_{10}\text{O}_{38}(\text{O}_2)_2] \cdot 2 \text{H}_2\text{O}$ (0.67 mM)/cyclooctene (0.1–1.0 M)/60% H_2O_2 (0.93 M)/ CH_3CN (30 ml) system at 69°C ; initial concentration of cyclooctene: 0.1 M (\square), 0.2 M (\bullet), 0.4 M (\blacksquare), 0.6 M (\circ), and 1.0 M (\blacktriangle).

amount and reaction time at the initial stage of the reaction, which allows us to estimate the initial rate (r) of product formation. The possibility that $[\text{Bu}_4\text{N}]_4[\text{Pr}^1\text{NH}_3]_2\text{H}[\text{PTi}_2\text{W}_{10}\text{O}_{38}(\text{O}_2)_2] \cdot 2 \text{H}_2\text{O}$ acts as an oxygen donor to form epoxide is ruled out, because none of epoxide was produced when the solution containing $[\text{Bu}_4\text{N}]_4[\text{Pr}^1\text{NH}_3]_2\text{H}[\text{PTi}_2\text{W}_{10}\text{O}_{38}(\text{O}_2)_2] \cdot 2 \text{H}_2\text{O}$ and cyclooctene in the absence of H_2O_2 was kept at 69°C within 48 h. As previously reported, $[\text{PTi}_2\text{W}_{10}\text{O}_{40}]^{7-}$ exhibited an induction period for the alkene oxidation due to the formation of η^2 -peroxo ligand at the TiO_6 site in the anion, and $[\text{PTi}_2\text{W}_{10}\text{O}_{38}(\text{O}_2)_2]^{7-}$ was the best as a catalyst for the alkene epoxidation by H_2O_2 compared to $[\text{PW}_{12}\text{O}_{40}]^{3-}$ and $[\text{PTi}_2\text{W}_{10}\text{O}_{40}]^{7-}$ [1]. The above results of Figs. 2–4 let us conclude that the coordination of alkene to the η^2 - O_2 ligand of $[\text{PTi}_2\text{W}_{10}\text{O}_{38}(\text{O}_2)_2]^{7-}$ (Eq. (1)) is the first step for the alkene epoxidation by H_2O_2 . $[\text{PW}_{12}\text{O}_{40}]^{3-}$ in the biphasic system was degraded to both η^2 - and $(\eta^2:\eta^1)$ -peroxo-containing $[(\text{PO}_4)\text{W}_4\text{O}_4(\text{O}_2)_8]^{3-}$ species, which was an active catalyst for the epoxidation [11–19]. Therefore, such a peroxo-containing $[(\text{PO}_4)\text{W}_4\text{O}_4(\text{O}_2)_8]^{3-}$ species seems also to require the alkene coordination to peroxo ligand for the epoxidation. Fig. 6 shows IR spectra of the yellow-colored solids after 24-h reaction at 69°C for the $[\text{Bu}_4\text{N}]_4[\text{Pr}^1\text{NH}_3]_2\text{H}[\text{PTi}_2\text{W}_{10}\text{O}_{38}(\text{O}_2)_2] \cdot 2 \text{H}_2\text{O}$ (0.67 mM)/cyclooctene (0.1 M)/60% H_2O_2 (0.93 M)/ CH_3CN (30 ml) system (A) and for the $[\text{Bu}_4\text{N}]_4[\text{Pr}^1\text{NH}_3]_2\text{H}[\text{PTi}_2\text{W}_{10}\text{O}_{38}(\text{O}_2)_2] \cdot 2 \text{H}_2\text{O}$ (0.67 mM)/60% H_2O_2 (0.93 M)/ CH_3CN (30 ml) system (B) which were isolated from turbid solutions due to water's content increased as a result of the reactions. IR spectrum of $[\text{Bu}_4\text{N}]_4[\text{Pr}^1\text{NH}_3]_2\text{H}[\text{PTi}_2\text{W}_{10}\text{O}_{38}(\text{O}_2)_2] \cdot 2 \text{H}_2\text{O}$ before reaction (C) is added in Fig. 6 for comparison. There is no significant change in the ratio of the intensity of $\nu_{\text{W-O}}$

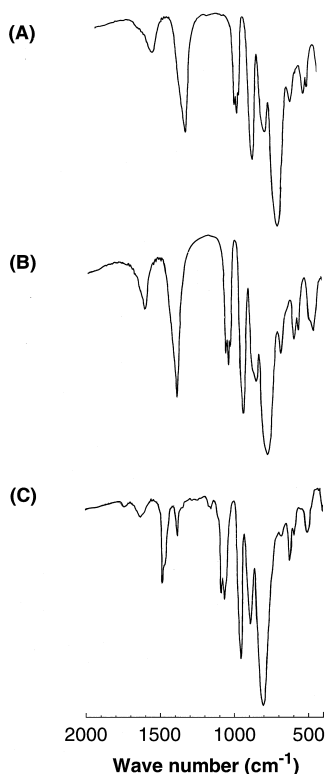


Fig. 6. IR spectra of $[\text{Bu}_4\text{N}]_4[\text{Pr}^{\text{I}}\text{NH}_3]_2\text{H}[\text{PTi}_2\text{W}_{10}\text{O}_{38}(\text{O}_2)_2] \cdot 2 \text{H}_2\text{O}$ solids after 24-h cyclooctene oxidation at 69°C (A) and 24-h H_2O_2 dismutation at 69°C in the absence of cyclooctene (B), and before reaction (C).

and $\nu_{\text{P-O}}$ frequencies at $600\text{--}1100 \text{ cm}^{-1}$ among IR spectra (A)–(C). However, some of the cations may be altered after epoxidation and H_2O_2 dismutation, since IR patterns at $1300\text{--}1700 \text{ cm}^{-1}$ slightly changed by the reactions. ^{31}P NMR spectrum of the yellow solids precipitated after 24-h reaction at 69°C for the $[\text{Bu}_4\text{N}]_4[\text{Pr}^{\text{I}}\text{NH}_3]_2\text{H}[\text{PTi}_2\text{W}_{10}\text{O}_{38}(\text{O}_2)_2] \cdot 2 \text{H}_2\text{O}$ (0.67 mM)/cyclooctene (0.1 M)/60% H_2O_2 (0.93 M)/ CH_3CN (30 ml) system was similar to the spectrum of $[\text{Pr}^{\text{I}}\text{NH}_3]_6\text{H}[\text{PTi}_2\text{W}_{10}\text{O}_{38}(\text{O}_2)_2] \cdot \text{H}_2\text{O}$ before reaction, as shown in Fig. 7 where each spectrum was measured in D_2O . The results of IR and ^{31}P NMR spectra indicate that there is no significant degradation of $[\text{PTi}_2\text{W}_{10}\text{O}_{38}(\text{O}_2)_2]^{7-}$ during the reaction, although formation of fragments at low concentrations can not be of course entirely excluded due to the limited sensitivity of the ^{31}P NMR method. The remaining solution after separation of the yellow solids for the 24-h reaction was concentrated to about 1/8 volume under the reduced pressure at 60°C with an accompanying rigorous oxygen-evolution and diluted by CD_3CN for ^{31}P NMR measurement. Fig. 8 shows ^{31}P NMR spectrum of this concentrated solution. As shown in Fig. 8 two ^{31}P NMR resonances with 2:1 intensity ratio are at $\delta -4.0$ (with $\nu_{1/2} = 2.2 \text{ Hz}$) and -11.0 (with $\nu_{1/2} = 4.4 \text{ Hz}$) probably due to $[(\text{PO}_4)\text{W}_4\text{O}_4(\text{O}_2)_8]^{3-}$ (at approximately $\delta -3.5$ in CDCl_3) [15] and $[\text{PTi}_2\text{W}_{10}\text{O}_{38}(\text{O}_2)_2]^{7-}$, respectively. In conjunction with high turnover (122) for the epoxidation (Table 1), this suggests that the decomposition of $[\text{PTi}_2\text{W}_{10}\text{O}_{38}(\text{O}_2)_2]^{7-}$ to the lower peroxo-species by self-oxidation throughout the alkene epoxidation is minor. Thus, the possibility of the participation of the lower tungstophosphates in the epoxidation was considered to be small.

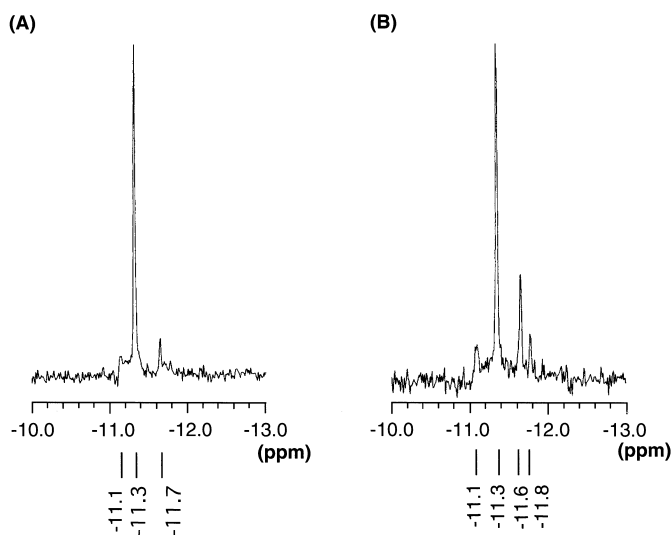


Fig. 7. ^{31}P NMR spectra of the yellow solids precipitated after 24-h reaction at 69°C for the $[\text{Bu}_4\text{N}]_4[\text{Pr}^{\text{I}}\text{NH}_3]_2\text{H}[\text{PTi}_2\text{W}_{10}\text{O}_{38}(\text{O}_2)_2] \cdot 2\text{H}_2\text{O}$ (0.67 mM)/cyclooctene (0.1 M)/60% H_2O_2 (0.93 M)/ CH_3CN (30 ml) system (A) and 55 mM $[\text{Pr}^{\text{I}}\text{NH}_3]_6\text{H}[\text{PTi}_2\text{W}_{10}\text{O}_{38}(\text{O}_2)_2] \cdot \text{H}_2\text{O}$ before reaction in D_2O .

3.3. Rate law

The reaction orders for catalyst, cyclooctene, and H_2O_2 were calculated from the slope of a log (r = observed rate at initial stage of reaction) against log (initial concentrations of catalyst, cyclooctene, and H_2O_2) for both reactions of epoxide and oxygen generation. The results for the

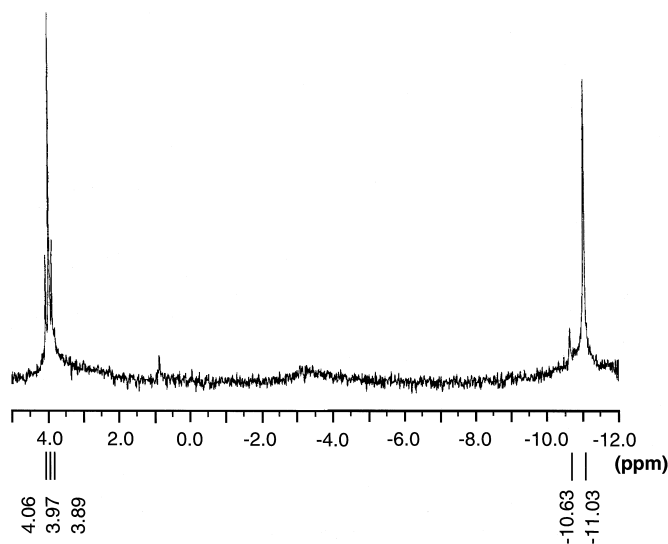


Fig. 8. ^{31}P NMR spectrum of the concentrated products in the remaining solution after separation of the yellow solids for the 24-h epoxidation. The yellow solids were precipitated after 24-h reaction at 69°C for the $[\text{Bu}_4\text{N}]_4[\text{Pr}^{\text{I}}\text{NH}_3]_2\text{H}[\text{PTi}_2\text{W}_{10}\text{O}_{38}(\text{O}_2)_2] \cdot 2\text{H}_2\text{O}$ (0.67 mM)/cyclooctene (0.1 M)/60% H_2O_2 (0.93 M)/ CH_3CN (30 ml) system, and the remaining solution rigorously reacted accompanied by oxygen-evolution on a concentration to about 1/8 volume under the reduced pressure at 60°C , then diluted by CD_3CN for the ^{31}P NMR measurement.

epoxide and oxygen generation are shown in Figs. 9 and 10, respectively. The dependences of concentrations of catalyst, H_2O_2 , and cyclooctene on the rate law of the epoxide generation are 0.9 ± 0.1 , 2.3 ± 0.1 , and 0.9 ± 0.2 , respectively. The dependences of concentrations of catalyst, H_2O_2 , and cyclooctene on the initial rate of oxygen generation in the presence of cyclooctene are 0.8 ± 0.1 , 1.5 ± 0.1 , and $-(0.9 \pm 0.1)$, respectively. The result of the initial rates of oxygen generation in the absence of cyclooctene is shown in Fig. 11 where the dependences in the rate law are 0.94 ± 0.04 for catalyst and 1.1 ± 0.1 for H_2O_2 . Thus, the kinetic measurements for epoxide and oxygen generation can be summarized by Eqs. (4)–(6) including rate constants (k):

$$d[\text{epoxide}]/dt = k_4[\text{catalyst}]^{0.9 \pm 0.1} \cdot [\text{H}_2\text{O}_2]^{2.3 \pm 0.1} \cdot [\text{cyclooctene}]^{0.9 \pm 0.2} \quad (4)$$

$$d[\text{O}_2]/dt = k_5[\text{catalyst}]^{0.8 \pm 0.1} \cdot [\text{H}_2\text{O}_2]^{1.5 \pm 0.1} \cdot [\text{cyclooctene}]^{-(0.9 \pm 0.1)} \quad (5)$$

$$d[\text{O}_2]/dt(\text{in the absence of cyclooctene}) = k_6[\text{catalyst}]^{0.94 \pm 0.04} \cdot [\text{H}_2\text{O}_2]^{1.1 \pm 0.1} \quad (6)$$

Multi orders in H_2O_2 dependence have also been assessed in both the alkene epoxidation (~ 2.8) with aryldiazonium-salt of $[\text{PTi}_x\text{W}_{12-x}\text{O}_{40-x}(\text{O}_2)_x]^{(3+2x)-}$ ($x = 1$ and 2) [1] and the allylic epoxidation (~ 1.4) with $[(\text{SiNb}_3\text{W}_9\text{O}_{37})_2\text{O}_3]^{7-}$ [24], indicating that H_2O_2 participates in the generation of the active catalyst prior to the rate determining step of the epoxidation.

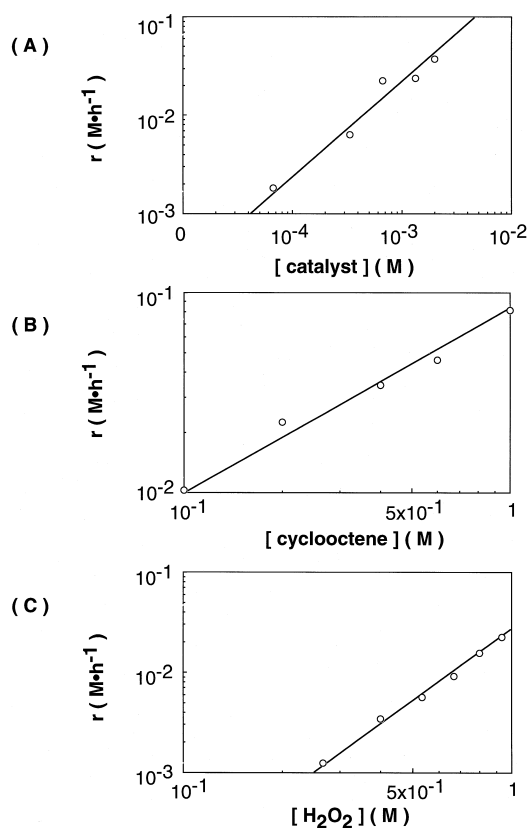


Fig. 9. Plots of $\log(r = \text{observed rate at initial stage of epoxide generation})$ against $\log(\text{initial concentrations of catalyst (A), cyclooctene (B), and } \text{H}_2\text{O}_2 \text{ (C)})$. Reaction conditions are 0.07–2.0 mM catalyst, 0.2 M cyclooctene, and 0.93 M H_2O_2 for (A) and 0.67 mM catalyst, 0.1–1.0 M cyclooctene, and 0.93 M H_2O_2 for (B), and 0.67 mM catalyst, 0.2 M cyclooctene, and 0.27–0.93 M H_2O_2 for (C) at 69°C in 30 ml CH_3CN .

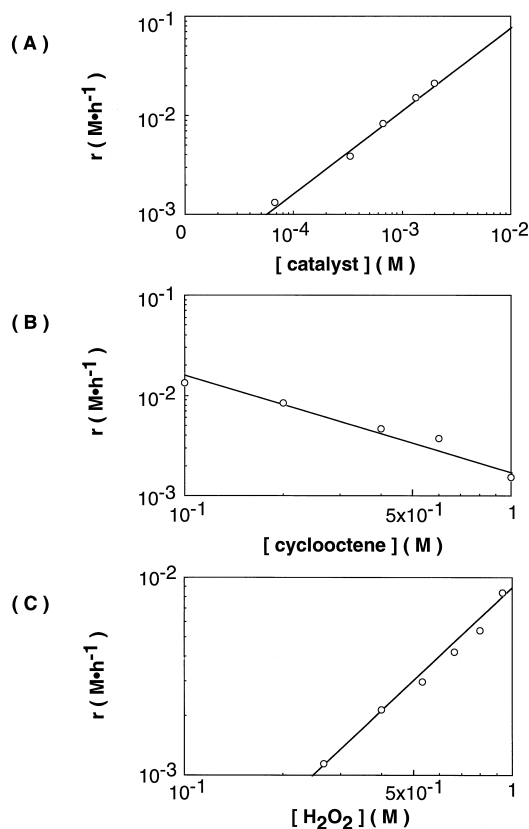
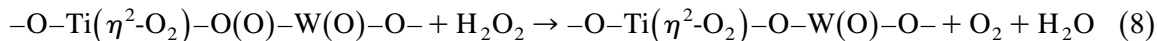
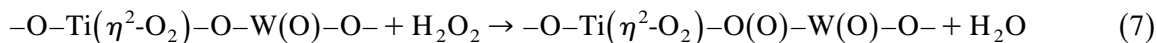


Fig. 10. Plots of $\log(r = \text{observed rate at initial stage of oxygen generation})$ against $\log(\text{initial concentrations of catalyst (A), cyclooctene (B), and H}_2\text{O}_2 \text{ (C)})$. Reaction conditions are the same as in Fig. 6.

$[\text{PTi}_2\text{W}_{10}\text{O}_{40}]^{7-}$ reacts with H_2O_2 to yield $[\text{PTi}_2\text{W}_{10}\text{O}_{38}(\text{O}_2)_2]^{7-}$ as a final product [20]. The reaction kinetics (Eq. (6)) of the $[\text{Bu}_4\text{N}]_4[\text{Pr}^{\text{I}}\text{NH}_3]_2\text{H}[\text{PTi}_2\text{W}_{10}\text{O}_{38}(\text{O}_2)_2] \cdot 2 \text{H}_2\text{O}$ -catalyzed dismutation of H_2O_2 in the absence of cyclooctene, therefore, implies the following scheme based on the catalytic stability of $[\text{PTi}_2\text{W}_{10}\text{O}_{38}(\text{O}_2)_2]^{7-}$:



where $-\text{O}-\text{Ti}(\eta^2-\text{O}_2)-\text{O}(\text{O})-\text{W}(\text{O})-\text{O}-$ denotes additional peroxidation with a mode of either $\eta^2:\eta^1-\text{O}_2$ for the bridging oxygen atom or $\eta^2-\text{O}_2$ for the terminal oxygen at the WO_6 site, probably with the mode similar to the $\eta^2-\text{O}_2$ peroxidation at the TiO_6 site of $[\text{PTi}_2\text{W}_{10}\text{O}_{40}]^{7-}$ by H_2O_2 .

For the steady-state conditions

$$\begin{aligned} d[\text{O}_2]/dt &= k_7[-\text{O}-\text{Ti}(\eta^2-\text{O}_2)-\text{O}-\text{W}(\text{O})-\text{O}-] \cdot [\text{H}_2\text{O}_2] \\ &= k_8[-\text{O}-\text{Ti}(\eta^2-\text{O}_2)-\text{O}(\text{O})-\text{W}(\text{O})-\text{O}-] \cdot \text{H}_2\text{O}_2 \end{aligned} \quad (9)$$

The dismutation of H_2O_2 is competitive with the epoxidation in the presence of cyclooctene as shown in Table 1. To explain the multi-order kinetics data (Eqs. (4) and (5)) in the H_2O_2 dependence for the monophasic $[\text{Bu}_4\text{N}]_4[\text{Pr}^{\text{I}}\text{NH}_3]_2\text{H}[\text{PTi}_2\text{W}_{10}\text{O}_{38}(\text{O}_2)_2] \cdot 2 \text{H}_2\text{O}/\text{cyclooctene}/\text{H}_2\text{O}_2/\text{CH}_3\text{CN}$

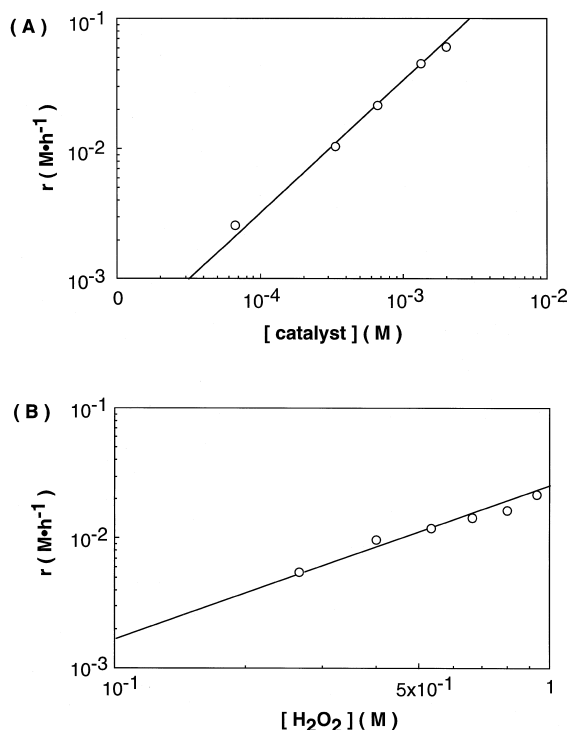
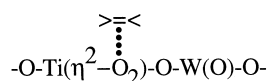
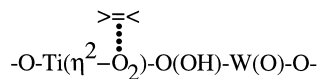


Fig. 11. Plots of $\log (r = \text{observed rate at initial stage of oxygen generation in the absence of cyclooctene})$ against \log (initial concentrations of catalyst (A) and H_2O_2 (B)). Reaction conditions are 0.07–2.0 mM catalyst and 0.93 M H_2O_2 for (A) and 0.67 mM catalyst and 0.27–0.93 M H_2O_2 for (B) at 69°C in 30 ml CH_3CN .

system, a branching chain scheme which involves formation of two kinds of hydroperoxo-catalyst intermediates is proposed: based on our conclusion that the alkene coordination to the $\eta^2\text{-O}_2$ ligand at the TiO_6 site precedes the epoxidation (Figs. 2–4), the alkene-coordinated catalyst



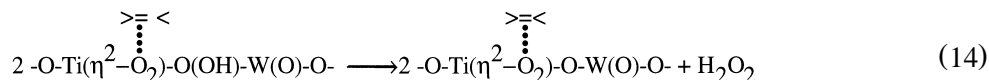
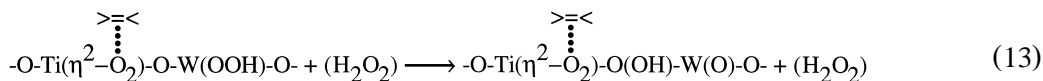
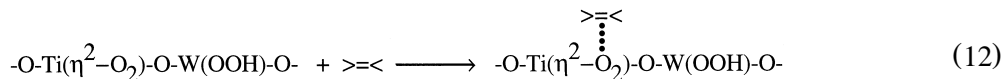
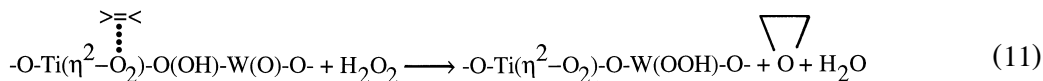
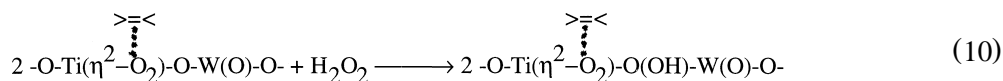
reacts with H_2O_2 to yield a hydroperoxo species



(Eq. (10)) as initiation for the branching chain scheme, followed by its reaction with H_2O_2 to epoxide

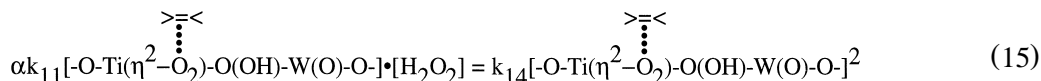


and other hydroperoxo species $-\text{O}-\text{Ti}(\eta^2-\text{O}_2)-\text{O}-\text{W}(\text{OOH})-\text{O}-$ (Eq. (11)).



Here Eq. (14) is a back reaction of Eq. (10).

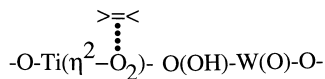
In steady-state conditions



and the reaction rate for the epoxidation is practically equal to that of chain propagation

$$\begin{aligned} d[\text{epoxide}]/dt &= k_{11} [\begin{array}{c} >= < \\ \vdots \\ -O-Ti(\eta^2-O_2)-O(OH)-W(O)-O- \end{array}] \cdot [H_2O_2] \\ &= (\alpha k_{11}^2/k_{14}) [H_2O_2]^2 \end{aligned} \quad (16)$$

where α is overall probability of conversion of $-O-Ti(\eta^2-O_2)-O-W(OOH)-O-$ into



for Eqs. (12) and (13). The former is tentatively assumed to be hydroperoxidation intermediate on the $W=O$ terminal oxygen atom and the latter on the bridging oxygen atom. Since α would be proportional to the concentrations of catalyst and alkene (Eq. (12)), the rate of epoxide formation under steady state conditions (Eq. (16)) can be described by a kinetic expression

$$d[\text{epoxide}]/dt = (\alpha' k_{11}^2/k_{14}) [\text{catalyst}] \cdot [H_2O_2]^2 \cdot [\text{cyclooctene}] \quad (17)$$

where α' is constant. Eq. (17) seems to outline the experimental data (Eq. (4)), in which more than two multi-order (2.3) dependence on H_2O_2 concentration implies a partial participation of H_2O_2 in the internal conversion between two hydroperoxotungstate intermediates (Eq. (13)).

Assuming that oxygen generation results from the reaction of $-\text{O}-\text{Ti}(\eta^2-\text{O}_2)-\text{O}(\text{O})-\text{W}(\text{O})-\text{O}-$ with H_2O_2 (Eqs. (7) and (8)) irrespective of cyclooctene, then the rate of the oxygen generation is

$$\begin{aligned} d[\text{O}_2]/dt &= k_8[-\text{O}-\text{Ti}(\eta^2-\text{O}_2)-\text{O}(\text{O})-\text{W}(\text{O})-\text{O}-] \cdot [\text{H}_2\text{O}_2] = k_7[-\text{O}-\text{Ti}(\eta^2-\text{O}_2)-\text{O}-\text{W}(\text{O})-\text{O}-] \cdot [\text{H}_2\text{O}_2] \\ &= (k_7/K) [-\text{O}-\text{Ti}(\overset{\text{>}}{\underset{\text{<}}{\text{O}}}-\text{O}_2)-\text{O}-\text{W}(\text{O})-\text{O}-] \cdot [\text{H}_2\text{O}_2] \cdot [\text{cyclooctene}]^{-1} \end{aligned} \quad (18)$$

Eq. (18) is in agreement with the experimental data on the dependence of cyclooctene and catalyst concentrations under conditions of a large excess of cyclooctene compared to catalyst. However, disagreement with the experimental data on the H_2O_2 concentration dependence (Eq. (5)) remains.

The above proposed scheme is based on the idea that the reaction pathway of the catalyst with H_2O_2 is altered by the coordination of alkene: the $\text{Ti}(\eta^2-\text{O}_2)\text{O}_5$ site is an active site for the H_2O_2 dismutation with an involvement of a peoxo intermediate (Eqs. (7) and (8)). On the other hand, the coordination of cyclooctene at the $\text{Ti}(\eta^2-\text{O}_2)\text{O}_5$ site modifies the electronic structure of surrounding sites as an active site for the epoxidation with an involvement of different peoxo intermediates (Eqs. (10) and (11)). The electronic modification of catalyst by the alkene coordination may be rationalized by change of pattern of the cyclic voltammogram of catalyst in the presence of cyclooctene which exhibited a positive potential shift (of about 0.1 V) (curve B in Fig. 4). Further work such as attempts to characterize the peoxo intermediates postulated in the branching chain mechanism will be carried out in order to substantiate the reaction pathways of $[\text{PTi}_2\text{W}_{10}\text{O}_{38}(\text{O}_2)_2]^{7-}$ catalyst.

Acknowledgements

We acknowledge a Grand-in-Aid for Scientific Research, Number 09218220, for the Ministry of Education, Science, Sports, and Culture for support of this work.

References

- [1] T. Yamase, E. Ishikawa, Y. Asai, S. Kanai, *J. Mol. Catal.* 114 (1996) 237.
- [2] C.L. Hill, R.B. Brown Jr., *J. Am. Chem. Soc.* 108 (1986) 536.
- [3] C.L. Hill, C.M. Prosser-McCartha, *Coord. Chem. Rev.* 143 (1995) 407, and references cited.
- [4] R. Neuman, M. Gara, *J. Am. Chem. Soc.* 116 (1994) 5509.
- [5] C.M. Tourné, G.F. Tourné, F. Zonnenvijlle, *J. Chem. Soc. Dalton Trans.* (1991) 143.
- [6] X. Zhang, K. Sasaki, C.L. Hill, *J. Am. Chem. Soc.* 118 (1996) 4809.
- [7] R. Neuman, M. Gara, *J. Am. Chem. Soc.* 117 (1995) 5066.
- [8] R. Neumann, A.M. Khenkin, *Inorg. Chem.* 34 (1995) 5753.
- [9] X. Zhang, Q. Chen, D.C. Duncan, C.F. Campana, C.L. Hill, *Inorg. Chem.* 36 (1997) 4207.
- [10] C. Venturello, R. D'Aloisio, J.C.J. Bart, M. Ricci, *J. Mol. Catal.* 32 (1985) 107.
- [11] C. Venturello, E. Alneri, M. Ricci, *J. Org. Chem.* 48 (1980) 1604.
- [12] C. Venturello, R. D'Aloisio, *J. Org. Chem.* 53 (1988) 1553.
- [13] Y. Ishii, K. Yamawaki, T. Yoshida, T. Ura, T. Ogawa, *J. Org. Chem.* 52 (1987) 1686.

- [14] Y. Ishii, K. Yamawaki, T. Ura, H. Yamada, T. Yoshida, T. Ogawa, *J. Org. Chem.* 53 (1988) 3587.
- [15] A.C. Dengel, W.P. Griffith, B.C. Parkin, *J. Chem. Soc. Dalton Trans.* (1993) 2683.
- [16] D.C. Duncan, R.C. Chambers, E. Hecht, C.L. Hill, *J. Am. Chem. Soc.* 117 (1995) 681.
- [17] C. Aubry, G. Chottard, N. Platzer, J.-M. Brégeault, R. Thouvenot, F. Chauveau, C. Huet, H. Ledon, *Inorg. Chem.* 30 (1991) 4409.
- [18] L. Salles, C. Aubry, R. Thouvenot, F. Robert, C. Dorémieux-Morin, G. Chottard, H. Ledon, Y. Jeannin, J.-M. Brégeault, *Inorg. Chem.* 33 (1994) 871.
- [19] M. Schwegler, M. Eloor, H. van Bekkum, *Tetrahedron Lett.* 29 (1988) 823.
- [20] T. Yamase, T. Ozeki, S. Motomura, *Bull. Chem. Soc. Jpn.* 65 (1992) 1453.
- [21] P.T. Domaille, W.H. Knoth, *Inorg. Chem.* 22 (1983) 818.
- [22] J.A.A. Ketelaar, C. van de Stolpe, A. Goudsmit, W. Dzcubas, *Rec. Trav. Chim.* 71 (1962) 1104.
- [23] T. Yamase, M. Sugeta, *Inorg. Chim. Acta* 172 (1990) 131.
- [24] M.W. Droege, R.G. Finke, *J. Mol. Catal.* 69 (1991) 323.